TUDelft

Delft University of Technology

Taylor least squares reconstruction technique for material point methods

Wobbes, E. D.; Möller, M.; Galavi, V.; Vuik, C.

Citation (APA)
Wobbes, E. D., Möller, M., Galavi, V., & Vuik, C. (2020). Taylor least squares reconstruction technique for material point methods. In R. Owen, R. de Borst, J. Reese, & C. Pearce (Eds.), *Proceedings of the 6th European Conference on Computational Mechanics: Solids, Structures and Coupled Problems, ECCM 2018 and 7th European Conference on Computational Fluid Dynamics, ECFD 2018* (pp. 806-817). (Proceedings of the 6th European Conference on Computational Mechanics: Solids, Structures and Coupled Problems, ECCM 2018 and 7th European Conference on Computational Fluid Dynamics, ECFD 2018). International Centre for Numerical Methods in Engineering, CIMNE.

Important note
To cite this publication, please use the final published version (if applicable).
Please check the document version above.

TAYLOR LEAST SQUARES RECONSTRUCTION TECHNIQUE FOR MATERIAL POINT METHODS

E. D. WOBBES[1], M. MÖLLER[1], V. GALAVI[2], AND C. VUIK[1]

[1] Department of Applied Mathematics, Delft University of Technology,
Van Mourik Broekmanweg 6, 2628 XE Delft, The Netherlands
{E.D.Wobbes, M.Moller, C.Vuik}@tudelft.nl

[2] Geo-Engineering section, Deltares
Boussinesqweg 1, 2629 HV Delft, The Netherlands
Vahid.Galavi@deltares.nl

Key words: Material Point Method, Function reconstruction, Least-squares approximation, Taylor basis, Dual domain, B-spline

Abstract. The material point method (MPM) is an effective computational tool for simulating problems involving large deformations. However, its direct mapping of the material-point data to the background grid frequently leads to severe inaccuracies. The standard function reconstruction techniques can considerably decrease these errors, but do not always guarantee the conservation of the total mass and linear momentum as the MPM algorithm does. In this paper, we introduce a novel technique, called Taylor Least Squares (TLS), which combines the Least Squares approximation with Taylor basis functions to reconstruct functions from scattered data. Within each element, the TLS technique approximates quantities of interest, such as stress and density, and when used with a suitable quadrature rule, it conserves the total mass and linear momentum after mapping the material-point information to the grid. The numerical and physical properties of the reconstruction technique are first illustrated on one- and two-dimensional functions. Then the TLS technique is tested as part of MPM, Dual Domain Material Point Method (DDMPM), and B-spline MPM (BSMPM) on a one-dimensional problem experiencing small and large deformations. The obtained results show that applying the TLS approximation significantly improves the accuracy of the considered versions of the material point method, while preserving the physical properties of the standard MPM.

1 INTRODUCTION

The material point method (MPM) [1, 2] is a computational tool for simulating problems involving large deformations. Despite its good performance in the occurrence of complex engineering studies, MPM has some numerical shortcomings. For example, when large strains are considered, the direct mapping of material-point data to the background grid can lead to considerable inaccuracies [3]. In addition, unphysical oscillations, known as grid-crossing errors, arise when particles travel between the elements [4].

Methods such as the Dual Domain Material Point method (DDMPM)[5] and B-Spline MPM (BSMPM) [6, 7] smoothen the gradients of the basis functions thereby reducing the grid-crossing error. Moreover, Sulsky and Gong [3], and Tielen et al. [7] have shown that advanced function reconstruction techniques can significantly decrease the quadrature errors within MPM and BSMPM. However, in contrast to the original MPM approach, standard reconstruction techniques do not necessarily conserve the mass and linear momentum of the system.

In this paper, we propose a novel reconstruction technique, called the Taylor Least Squares (TLS), that combines Least Squares approximation with local Taylor basis functions [8]. For each element, it reconstructs quantities of interest, such as stress and density, from the particle data. The functions are evaluated at the integration points and Gauss quadrature is applied to determine the internal forces and velocities at the degrees of freedom (DOFs). If each element contains a sufficient number of Gauss points, the proposed mapping approach preserves the total mass and linear momentum.

First, the numerical and physical properties of the TLS reconstruction are illustrated without including it in the MPM algorithm. After that, the reconstruction technique is applied within MPM, DDMPM, and BSMPM for a time-dependent one-dimensional problem under small and large deformations. The obtained results show that TLS reconstruction leads to a conservative projection, while significantly decreasing the spatial errors and improving the convergence behaviour of the considered material point methods.

This paper is structured as follows. Section 2 introduces the main concepts of the TLS reconstruction and demonstrates its performance for one- and two-dimensional functions. Section 3 outlines the use of the technique within the MPM algorithm. Section 4 gives a formal analysis of its conservative properties. Section 5 describes the performance of MPM, DDMPM, and BSMPM with the TLS reconstruction based on a one-dimensional problem that undergoes small and large deformations. Section 6 provides the conclusions.

2 TAYLOR LEAST SQUARES RECONSTRUCTION

Let $\{\mathbf{x}_p\}_{p=1}^{N_p}$ be a set of N_p distinct data points from $\mathbb{R}^n$ with $n = \{1, 2\}$ and $\{u(\mathbf{x}_p)\}_{p=1}^{N_p}$ contain the corresponding values. It is assumed that $u \in F$, where F is a normed function space on $\mathbb{R}$, and $P = \text{span}\{\psi_i\}_{i=1}^{n_b} \subset F$ is a set of n_b basis functions. Defining the basis function vector $\boldsymbol{\psi}(\mathbf{x}) = [\psi_1(\mathbf{x}) \ \psi_2(\mathbf{x}) \ \ldots \ \psi_{n_b}(\mathbf{x})]^T$, and vector of coefficients $\mathbf{a} = [a_1 \ a_2 \ \ldots \ a_{n_b}]^T$, the Least Squares [9] approximation at a point $\mathbf{x} \in \mathbb{R}^n$ is the value

$\hat{u} \in P$ given by

$$\hat{u}(\mathbf{x}) = \sum_{i=1}^{n_b} a_i \psi_i(\mathbf{x}) = \boldsymbol{\psi}^T(\mathbf{x})\mathbf{a} \quad \text{with} \quad \mathbf{a} = D^{-1}BU, \tag{1}$$

where

$$D = \sum_{p=1}^{N_p} \boldsymbol{\psi}(\mathbf{x}_p)\boldsymbol{\psi}^T(\mathbf{x}_p), \; B = [\boldsymbol{\psi}(\mathbf{x}_1) \; \boldsymbol{\psi}(\mathbf{x}_2) \; \dots \; \boldsymbol{\psi}(\mathbf{x}_{N_p})], \; U = [u(\mathbf{x}_1) \; u(\mathbf{x}_2) \; \dots \; u(\mathbf{x}_{N_p})]^T.$$

The basis for P can be constructed from local Taylor basis functions [8]. To define these basis functions we introduce the concept of the volume average. For a generic function f, the volume average over Ω_e is equal to $\overline{f} = \frac{1}{|\Omega_e|} \int_{\Omega_e} f \, d\Omega_e$, where $|\Omega_e|$ is the volume of cell e (i.e., in one dimension, $\Omega_e = [x_{min}, x_{max}]$ with $x_{max} > x_{min}$, and $|\Omega_e| = x_{max} - x_{min}$).

The Taylor basis functions are then given by [8]

$$\psi_1 = 1, \;\; \psi_2 = \frac{x - x_c}{\Delta x}, \;\; \psi_3 = \frac{y - y_c}{\Delta y}, \;\; \psi_4 = \frac{(x - x_c)^2}{2\Delta x^2} - \frac{\overline{(x - x_c)^2}}{2\Delta x^2},$$

$$\psi_5 = \frac{(y - y_c)^2}{2\Delta y^2} - \frac{\overline{(y - y_c)^2}}{2\Delta y^2}, \;\; \psi_6 = \frac{(x - x_c)(y - y_c) - \overline{(x - x_c)(y - y_c)}}{\Delta x \Delta y}.$$

Here, $x_c = \frac{x_{max} + x_{min}}{2}$, $y_c = \frac{y_{max} + y_{min}}{2}$, $\Delta x = \frac{x_{max} - x_{min}}{2}$, and $\Delta y = \frac{y_{max} - y_{min}}{2}$.

An important quality of the Taylor basis that ensures the conservative properties of the reconstruction technique is the following:

$$\int_{\Omega_e} \psi_i \, d\Omega_e = \begin{cases} |\Omega_e| & \text{if } i = 1, \\ 0 & \text{if } i \neq 1. \end{cases} \tag{2}$$

Thus, if a function u has to be reconstructed so that its integral over Ω_e, $\int_{\Omega_e} u(\mathbf{x}) \, d\Omega_e = c$ ($c \in \mathbb{R}$), is preserved, the TLS approximation of u is equal to

$$u(\mathbf{x}) \approx \hat{u}(\mathbf{x}) = \sum_{i=1}^{n_b} a_i \psi_i(\mathbf{x}). \tag{3}$$

From Equation (2), it follows that:

$$\int_{\Omega_e} \hat{u}(\mathbf{x}) \, d\Omega_e = \int_{\Omega_e} \sum_{i=1}^{n_b} a_i \psi_i(\mathbf{x}) \, d\Omega_e = \sum_{i=1}^{n_b} a_i \int_{\Omega_e} \psi_i(\mathbf{x}) \, d\Omega_e = a_1 |\Omega_e|. \tag{4}$$

This implies that the reconstructed function $\hat{u}$ preserves the integral value if

$$a_1 = \frac{c}{|\Omega_e|}, \tag{5}$$

which can be enforced explicitly. In this case, the Least Squares reconstruction would be based on $n_b - 1$ basis functions.

2.1 Examples

First of all, we reconstruct a one-dimensional function $u(x) = \sin(x) + 2$ on $[0, 4\pi]$. The integral is equal to 8π, in this case. The domain is discretised by four elements of size π and contains two data points are located at π and in total 12 data points. In the first element, two data points are positioned at the edges and one in the interior. In the third cell, the data points are distributed uniformly. The remaining data points have random positions creating several types of data distribution within each element.
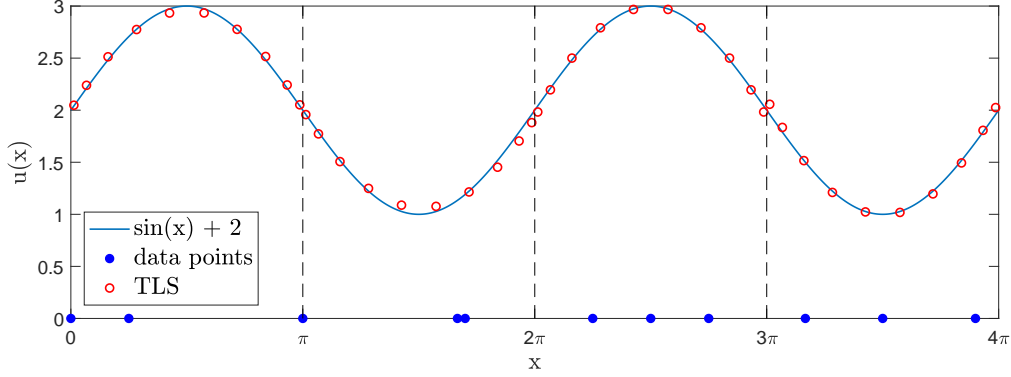

Figure 1: TLS reconstructions of $u(x) = \sin(x) + 2$ on $[0, 4\pi]$ for different types of data point distribution within an element.

The TLS approximation is produced using three Taylor basis functions. Figure 1 depicts the obtained results for 10 integration points per element. The overall performance of the TLS technique is quantified by the Root-Mean-Square (RMS) error for the function and the relative error for its integral. Both errors are calculated for 10 Gauss points within each element. The RMS error is equal to $3.8139 \cdot 10^{-2}$, whereas the relative error is equal to $7.0679 \cdot 10^{-16}$. When only two Gauss points per element are used, the relative error for the integral is equal to $2.7903 \cdot 10^{-15}$. Thus, for this example, the TLS approach preserves the integral up to machine precision.

Moreover, we reconstruct a two-dimensional function $u(x, y) = \sin(x) \cos(y)$ on $[0, 5] \times [0, 5]$. The corresponding integral is approximately equal to $-6.8691 \cdot 10^{-1}$. The domain is discretised by 1×1 quadrilateral elements. Each element contains 6 data points with x-coordinates equal to $x_{min} + \frac{1}{3}$ and $x_{max} - \frac{1}{3}$, and y-coordinates set to $y_{min} + \frac{1}{4}$, $\frac{y_{min} + y_{max}}{2}$, and $y_{max} - \frac{1}{4}$. This is illustrated in Figure 2.

This data distribution allows the use of six Taylor basis functions for the approximation. Four Gauss points per element were defined to compute the RMS and relative errors. The RMS error for the function is equal to $6.17 \cdot 10^{-3}$, while the relative error for the integral is equal to $6.6613 \cdot 10^{-16}$. The reconstruction is visualised in Figure 2.

3 INTEGRATION INTO MATERIAL POINT METHOD

When the TLS reconstruction technique is integrated into the material-point method or its more advanced version, such as DDMPM and BSMPM, particles serve as data points.
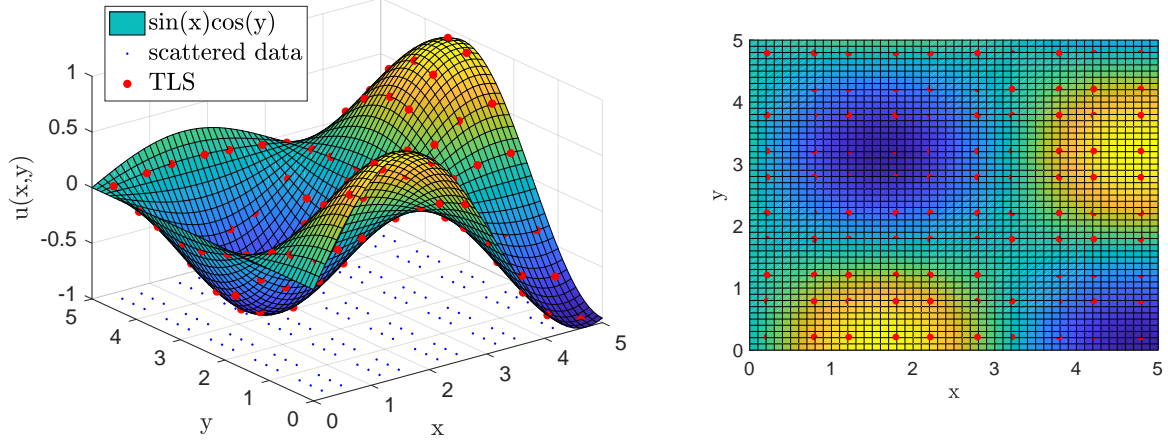
Figure 2: TLS reconstructions of $u(x, y) = \sin(x)\cos(y)$ on $[0, 5] \times [0, 5]$ using 6 data points within each element: side and top view.

To conserve the integral of a certain quantity within each element[1], the coefficient of the first basis function is specified according to Equation (5). The remaining coefficients are calculated from Equation (1) without ψ_1 so that the integral value is preserved. When the conservation is not required, a standard Least Squares approach is followed. This implies that all unknown coefficients are obtained from the Least Squares approximation. This section provides a more detailed description for one-dimensional problems.

First, the TLS reconstruction is applied to replace the MPM-integration in the internal force computation by an exact method, such as an element-wise Gauss quadrature. In the standard one-dimensional MPM algorithm, the internal forces at the DOFs are given by

$$\mathbf{f}^{\text{int}} = \sum_{p=1}^{N_p} \sigma_p \boldsymbol{\phi}'(x_p) V_p, \tag{6}$$

where $\mathbf{f}^{\text{int}}$ is the vector containing the internal forces at the DOFs, N_p is the total number of material points, σ_p is the particle stress, $\boldsymbol{\phi}(x) = [\phi_1(x)\ \phi_2(x)\ \phi_3(x)]^T$ is the vector of one-dimensional basis functions, x_p is the particle position, and V_p is the particle volume.

We propose replacing Equation (6) by the following computational procedure.

1. Apply a quadratic TLS technique to reconstruct the stress field from the particle data within each active element without explicitly specifying the coefficient of the first Taylor basis function:

$$\hat{\sigma}_e = \sum_{i=1}^{n_b} s_i \psi_i, \tag{7}$$

where $\hat{\sigma}_e$ is the stress in element e, s_i is the coefficient corresponding to the ith Taylor basis function. Outside of the considered element, $\hat{\sigma}_e$ is zero. The global

---

[1]For BSMPM, an element is defined as a non-empty knot span.

approximation of the stress function, $\hat{\sigma}$, is then equal to $\hat{\sigma} = \sum_{e=1}^{N_e} \hat{\sigma}_e$.

2. Integrate the stress approximation using a two-point Gauss quadrature:

$$\mathbf{f}^{\text{int}} \approx \int_\Omega \hat{\sigma}(x,t)\boldsymbol{\phi}' \, d\Omega = \sum_{g=1}^{N_g} \hat{\sigma}\left(x_g\right) \boldsymbol{\phi}'\left(x_g\right) \omega_g,$$

where N_g is the total number of Gauss points, x_g is the global position of a Gauss point, and ω_g is the weight of a Gauss point. To assure the exact integration of the approximated function N_g should be selected so that $n_b \leq \frac{2N_g}{N_e}$.

Within the widely used Modified-Update-Stress-Last (MUSL) scheme [2], the TLS technique should also be applied for the computation of the material-point velocities. In the standard MUSL calculation, the material-point velocities are directly mapped to the DOFs:

$$\mathbf{v} = M^{-1} \sum_{p=1}^{N_p} m_p \boldsymbol{\phi}\left(x_p\right) v_p, \tag{8}$$

where $\mathbf{v}$ is the vector containing the velocity at the DOFs, M is the mass matrix, m_p is the particle mass, and v_p is the particle velocity. The proposed mapping procedure has the following steps.

1. Apply a quadratic TLS approach to reconstruct the density field and the product of density and velocity within each active element ρ_e and $(\widehat{\rho v})_e$, respectively, while preserving the mass and momentum of the element:

$$\hat{\rho}_e = \sum_{i=1}^{n_b} r_i \psi_i \ \text{ with } \ r_1 = \frac{1}{|\Omega_e|} \sum_{\{p|x_p \in \Omega_e\}} m_p$$

$$(\widehat{\rho v})_e = \sum_{i=1}^{n_b} \gamma_i \psi_i \ \text{ with } \ \gamma_1 = \frac{1}{|\Omega_e|} \sum_{\{p|x_p \in \Omega_e\}} m_p v_p.$$

where r_i and γ_i are the coefficients corresponding to the ith Taylor basis function. Outside of element e, $\hat{\rho}_e$ and $(\widehat{\rho v})_e$ are zero. The global approximations are then equal to $\hat{\rho} = \sum_{e=1}^{N_e} \hat{\rho}_e$ and $(\widehat{\rho v}) = \sum_{e=1}^{N_e} (\widehat{\rho v})_e$.

2. Integrate the approximations using a two-point Gauss quadrature to obtain the momentum vector $\mathbf{p}$ and and the consistent mass matrix M^C:

$$\mathbf{p} = \sum_{g=1}^{N_g} (\widehat{\rho v})\left(x_g\right) \boldsymbol{\phi}\left(x_g\right) \omega_g, \tag{9}$$

$$M^C = \sum_{g=1}^{N_g} \hat{\rho}\left(x_g\right) \boldsymbol{\phi}\left(x_g\right) \left(\boldsymbol{\phi}\left(x_g\right)\right)^T \omega_g, \tag{10}$$

6

3. Compute the velocity vector:

$$\mathbf{v} = (M^C)^{-1}\mathbf{p}. \tag{11}$$

It should be noted that M^C may be replaced by a lumped mass matrix without a loss of conservative properties of the mapping procedure.

4   CONSERVATION OF MASS AND MOMENTUM

As mentioned in Section 3, the TLS technique uses the following approximations:

$$\rho_e \approx \hat{\rho}_e = \sum_{i=1}^{n_b} r_i \psi_i \text{ with } r_1 = \frac{1}{|\Omega_e|} \sum_{\{p|x_p \in \Omega_e\}} m_p$$

$$(\rho v)_e \approx (\widehat{\rho v})_e = \sum_{i=1}^{n_b} \gamma_i \psi_i \text{ with } \gamma_1 = \frac{1}{|\Omega_e|} \sum_{\{p|x_p \in \Omega_e\}} m_p v_p,$$

According to Equation (4) and (5), this preserves the mass $\mathcal{M}_e$ and momentum $\mathcal{P}_e$ of element e. As a result, the total mass and momentum of the system are conserved after the TLS reconstruction:

$$\mathcal{M} = \sum_{e=1}^{N_e} \mathcal{M}_e = \sum_{e=1}^{N_e} \sum_{\{p|x_p \in \Omega_e\}} m_p = \sum_{p=1}^{N_p} m_p, \tag{12}$$

$$\mathcal{P} = \sum_{e=1}^{N_e} \mathcal{P}_e = \sum_{e=1}^{N_e} \sum_{\{p|x_p \in \Omega_e\}} m_p v_p = \sum_{p=1}^{N_p} m_p v_p. \tag{13}$$

The mass- and momentum-conservation properties of the mapping obtained using TLS reconstruction and Gauss quadrature can be shown as well.

Since the total mass is equal to the sum of the entries in the consistent mass matrix from Equation (10), it can be written as

$$\mathcal{M} = \sum_{i=1}^{N_n} \sum_{j=1}^{N_n} M_{ij}^C = \sum_{i=1}^{N_n} \sum_{j=1}^{N_n} \sum_{g=1}^{N_g} \hat{\rho}(x_g) \phi_i(x_g) \phi_j(x_g) \omega_g$$

$$= \sum_{g=1}^{N_g} \hat{\rho}(x_g) \sum_{i=1}^{N_n} \phi_i(x_g) \sum_{j=1}^{N_n} \phi_j(x_g) \omega_g = \sum_{g=1}^{N_g} \hat{\rho}(x_g) \omega_g. \tag{14}$$

The last equality is derived using the partition of unity property of the considered basis functions (i.e., piecewise-linear and B-spline basis functions). In the remaining part of the proof, we assume that $n_b \leq \frac{2N_g}{N_e}$, so that the Gauss quadrature with $\frac{N_g}{N_e}$ integration points per element is exact. Therefore, the following holds:

$$\mathcal{M} = \sum_{g=1}^{N_g} \hat{\rho}(x_g) \omega_g = \sum_{e=1}^{N_e} \sum_{\{g|x_g \in \Omega_e\}} \hat{\rho}_e(x_g) \omega_g = \sum_{e=1}^{N_e} \int_{\Omega_e} \hat{\rho}_e \, d\Omega_e = \sum_{e=1}^{N_e} \mathcal{M}_e = \sum_{p=1}^{N_p} m_p.$$

The last two steps emerge from the conservation of mass per element and Equation (12).

For the linear momentum, we also assume that $n_b \leq \frac{2N_g}{N_e}$. Repeating the above steps, the total momentum after the mapping can be written as

$$
\begin{aligned}
\mathcal{P} &= \sum_{i=1}^{N_n} p_i = \sum_{i=1}^{N_n} \sum_{g=1}^{N_g} (\widehat{\rho v})(x_g)\phi_i(x_g)\omega_g = \sum_{g=1}^{N_g} (\widehat{\rho v})(x_g) \sum_{i=1}^{N_n} \phi_i(x_g)\omega_g \\
&= \sum_{g=1}^{N_g} (\widehat{\rho v})(x_g)\omega_g = \sum_{e=1}^{N_e} \sum_{\{g|x_g \in \Omega_e\}} (\widehat{\rho v})_e(x_g)\omega_g \\
&= \sum_{e=1}^{N_e} \int_{\Omega_e} (\widehat{\rho v})_e d\Omega_e = \sum_{e=1}^{N_e} \mathcal{P}_e = \sum_{p=1}^{N_p} m_p v_p.
\end{aligned}
$$

Therefore, we have shown that if the Gauss quadrature is performed using a sufficient number of integration points, the mass and momentum balance is satisfied not only by the TLS function reconstruction, but also by its combination with the Gauss quadrature.

5   NUMERICAL RESULTS

In this section, we consider a one-phase vibrating bar that undergoes small and large deformations. The material-point solutions in terms of the particle displacement, velocity, and stress are considered at the particle positions. For small deformations, the problem has an analytical solution that allows us to perform a spatial convergence analyses. The contribution of temporal errors is minimised by using small time-step sizes and short simulation times. For large strains, the analytical solution is not available. Thus, the numerical results are compared to the solution obtained with the Updated Lagrangian Finite Element Method (ULFEM) [10]. The conservative properties of the material point methods are quantified by calculating the maximum relative errors in the total mass and momentum over all time steps before and after the computation of the velocity at the DOFs. It should be noted that for MPM, DDMPM, and BSMPM, the errors in the mass and momentum are bounded by 10^{-15}. The TLS reconstruction technique is applied using three basis functions (i.e., $n_b = 3$).

The example describes the vibration of a one-phase bar with fixed ends. The motion is captured by the following partial differential equations:

$$
\rho\frac{\partial v}{\partial t} = \frac{\partial \sigma}{\partial x}, \quad \frac{\partial \sigma}{\partial t} = E\frac{\partial v}{\partial x}, \quad v = \frac{\partial u}{\partial t}.
$$

Here, ρ is the density, v is the velocity, σ is the stress, E is the Young's modulus, and u is the displacement. The vibration is triggered by an initial velocity that varies along the bar leading to the following initial and boundary conditions:

$$
u(x,0) = 0, \quad v(x,0) = v_0 \sin\left(\frac{\pi x}{H}\right), \quad \sigma(x,0) = 0, \quad u(0,t) = 0, \quad u(H,t) = 0,
$$

where H is the length of the bar and v_0 is the maximum initial velocity.

Table 1: Vibrating bar problem: exemplary parameters allowing for small deformations.

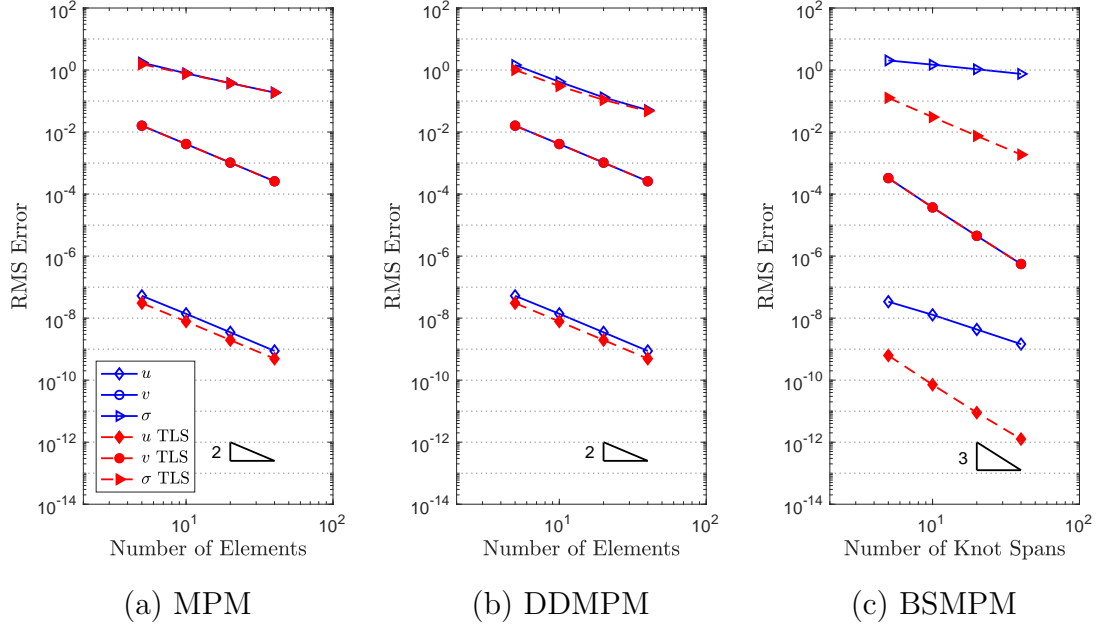| Parameter	Symbol	Value	Unit
Height	H	1.00	m
Density	ρ	$2.00 \cdot 10^3$	kg/m^3
Young's modulus	E	$7.00 \cdot 10^6$	Pa
Max. initial velocity	v_0	0.28	m/s^2

(a) MPM (b) DDMPM (c) BSMPM

Figure 3: Vibrating bar problem without grid crossing: spatial convergence of material point methods. The results are shown for the material point methods without TLS (solid blue line, empty marker) and with TLS reconstruction (red filled marker).

For small strains, the analytical solution in terms of displacement is given by

$$u(x,t) = \frac{v_0 H}{\pi \sqrt{E/\rho}} \sin\left(\frac{\pi \sqrt{E/\rho}\, t}{H}\right) \sin\left(\frac{\pi x}{H}\right), \tag{15}$$

The solutions for velocity and stress can be computed directly from Equation (15). Table 1 provides exemplary parameter values for the vibrating bar benchmark under small deformations. The time-step size and total simulation time are $1 \cdot 10^{-7}$ s and $1.9 \cdot 10^{-6}$ s, respectively. Furthermore, the number of elements is varied from 5 to 40, while the number of particles per cell (PPC) is fixed to 12. Grid crossing does not occur, and the maximal observed strain is equal to $5.3 \cdot 10^{-7}$ m.

The results in terms of spatial errors are shown in Figure 3. As expected, MPM with piecewise-linear basis functions demonstrates second-order convergence in both the displacement and velocity. Since the stress is not discretised, its convergence rate is one.

9

The application of the TLS reconstruction technique has almost no influence on the stress, but decreases the displacement error by a factor of 1.7. For DDMPM, the application of the reconstruction technique tends to reduce not only the error in the displacement, but also in the stress.

The use of quadratic B-spline basis functions leads to a significant decrease in the error and a higher order of convergence for the velocity, but causes problems at the boundaries of the domain for both stress and displacement. The large values of the error at the boundaries prevent the reduction of the RMS error and worsen the convergence properties of the method. However, the use of BSMPM with the function reconstruction technique eliminates the boundary issues. Consequently, third-order convergence is obtained for all the considered quantities. It should also be noted that the integration of the TLS reconstruction in BSMPM produces more accurate results than the other considered methods.

The errors produced by the TLS technique for the total mass and momentum remain close to machine precision. For example, when 40 elements with 12 PPC are used, the relative error in mass is equal to $7.5033 \cdot 10^{-15}$ for MPM, $7.3896 \cdot 10^{-15}$ for DDMPM, and $7.5033 \cdot 10^{-15}$ for BSMPM.

For large-deformation simulations, the parameters from Table 2 are used. The time-step size and the simulation time are increased to $1 \cdot 10^{-5}$ s and 0.1 s, respectively. The domain is discretised using 20 elements (knot spans) with initially 8 PPC. The maximal strain that is reached is 0.056 m.

Table 2: Vibrating bar problem: exemplary parameters allowing for large deformations.

Parameter	Symbol	Value	Unit
Height	H	1.00	m
Density	ρ	$2.00 \cdot 10^3$	kg/m^3
Young's modulus	E	$4.00 \cdot 10^4$	Pa
Max. initial velocity	v_0	0.80	m/s^2

In the standard MPM simulation, material points cross the element boundaries more than 450 times leading to significant inaccuracies in the results. Although grid crossing influences the computation of the displacement and velocity, its most evident consequences are in the stress distribution. DDMPM and BSMPM reduce the grid-crossing error, but their results still significantly deviate from the solution provided by ULFEM. This is shown in Figure 4.

Table 3: Maximum relative errors in the total mass $\mathcal{M}$ and momentum $\mathcal{P}$ over the simulation run with the TLS reconstruction when grid crossing occurs. The vibrating bar is discretised using 40 elements (knot spans) and 12 PPC.

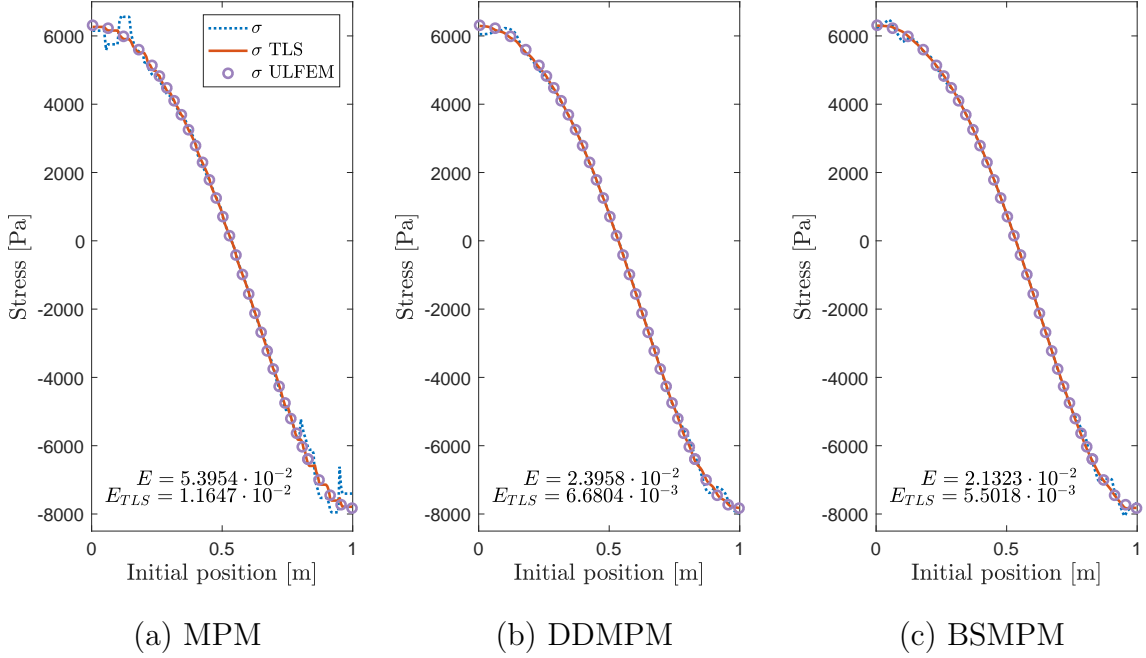| MPM		DDMPM		BSMPM	
Error$_{\mathcal{M}}$	Error$_{\mathcal{P}}$	Error$_{\mathcal{M}}$	Error$_{\mathcal{P}}$	Error$_{\mathcal{M}}$	Error$_{\mathcal{P}}$
$2.933 \cdot 10^{-14}$	$5.847 \cdot 10^{-15}$	$2.910 \cdot 10^{-14}$	$5.773 \cdot 10^{-15}$	$2.910 \cdot 10^{-14}$	$5.721 \cdot 10^{-15}$

Figure 4: Vibrating bar problem with grid crossing: stress distribution and corresponding relative errors in the L_2-norm. The results are obtained for the material point methods without reconstruction technique (dotted blue line) and ULFEM (grey circle marker).

The figure also illustrates that the application of the TLS approximation reconstruction leads to close agreement of the MPM, DDMPM, and BSMPM solutions with that of ULFEM. The maximal reduction of the relative error in L_2-norm made by standard MPM is achieved when the reconstruction technique is combined with BSMPM. More precisely, the integration of the TLS reconstruction in BSMPM decreases the MPM error by a factor of 9.8. With DDMPM, it reduces the MPM error by a factor of 8.1. The conservative properties of the reconstruction techniques are provided in Table 3.

6 CONCLUSIONS

In this paper, we have introduced Taylor Least Squares reconstruction for one- and two-dimensional functions. The proposed technique combines the Least Squares approximation with local Taylor basis functions to accurately reconstruct the quantities of interest from scattered particle data within each element. We have shown that within MPM the TLS approximation conserves the mass and linear momentum of the system after the material-point data is mapped to the integration points. More importantly, when used with a sufficiently accurate numerical quadrature rule, the technique preserves the total mass and momentum after the information is projected to the degrees of freedom of the grid.

For a one-dimensional example undergoing small and large deformations, the TLS

11

technique was applied within MPM, DDMPM, and BSMPM. Without grid crossing, the reconstruction technique had little influence on MPM, but was able to improve the convergence properties of DDMPM and BSMPM. When material points started to cross cell boundaries, the TLS approximation smoothened the solutions obtained by all considered material point methods and brought them closer to the solution computed by ULFEM. Therefore, the TLS reconstruction maintains the physical properties of the standard material point methods, while significantly improving their accuracy.

REFERENCES

[1] D Sulsky, Z Chen, and HL Schreyer. A particle method for history-dependent materials. *Comput Methods in Appl Mech Eng*, 118(1-2):179–196, 1994.

[2] D Sulsky, SJ Zhou, and HL Schreyer. Application of a particle-in-cell method to solid mechanics. *Comput Phys Commun*, 87(1–2):236–252, 1995.

[3] D Sulsky and M Gong. Improving the material-point method. Innovative Numerical Approaches for Multi-Field and Multi-Scale Problems, pages 217–240. Springer, 2016.

[4] SG Bardenhagen and EM Kober. The generalized interpolation material point method. *Comput Model Eng Sci*, 5(6):477–496, 2004.

[5] DZ Zhang, X Ma, and PT Giguere. Material point method enhanced by modified gradient of shape function. *J Comput Phys*, 230(16):6379–6398, 2011.

[6] M Steffen, RM Kirby, and M Berzins. Analysis and reduction of quadrature errors in the material point method. *Int J Numer Methods Eng*, 76(6):922–948, 2008.

[7] R Tielen, E Wobbes, M Möller, and L Beuth. A high order material point method. *Procedia Eng*, 175:265–272, 2017.

[8] H Luo, JD Baum, and R Löhner. A discontinuous Galerkin method based on a Taylor basis for the compressible flows on arbitrary grids. *J Comput Phys*, 227(20):8875–8893, 2008.

[9] AM Legendre. *Nouvelles méthodes pour la détermination des orbites des comètes*. F. Didot, 1805.

[10] KJ Bathe, E Ramm, and EL Wilson. Finite element formulations for large deformation dynamics analysis. *Int J Numer Methods Eng*, 9(2):353–386, 1975.